

Cite this: *Lab Chip*, 2012, **12**, 2487–2490

www.rsc.org/loc

## COMMUNICATION

# High-throughput immunoassay through in-channel microfluidic patterning†

Chunhong Zheng,<sup>ab</sup> Jingwen Wang,<sup>a</sup> Yuhong Pang,<sup>ab</sup> Jianbin Wang,<sup>a</sup> Wenbin Li,<sup>c</sup> Zigang Ge<sup>\*a</sup> and Yanyi Huang<sup>\*ab</sup>

Received 9th February 2012, Accepted 26th March 2012

DOI: 10.1039/c2lc40145b

We have developed an integrated microfluidic immunoassay chip for high-throughput sandwich immunoassay tests. The chip creates an array of reactive patterns through mechanical protection by actuating monolithically embedded button valves. We have demonstrated that this chip can achieve highly sensitive immunoassay tests within an hour, and requires only microliter samples.

Immunoassays, including enzyme-linked immunosorbent assays (ELISAs) and other related assays, are important techniques for biochemical analysis and diagnostic detection.<sup>1,2</sup> Traditional immunoassay experiments, carried out on multi-well plates, take several hours to complete because of the hour-long incubation time for most steps. Consumption issues also remain a challenge for tests with precious samples and antibody reagents. In addition, immunoassays usually require sophisticated instruments and skilful operations to obtain reliable results. Recently, the rapid development of microfluidic technologies, also known as “lab-on-a-chip” technologies, has enabled the miniaturization of various chemical or biochemical reactions onto tiny devices.<sup>3,4</sup> For immunoassays, microfluidic devices present great advantages, including decrease of consumption, reduction of experimental time, increasing of throughput, and convenient operation.<sup>5,6</sup> Methods utilizing capillary electrophoresis,<sup>7</sup> spinning CD-like disks,<sup>8</sup> and magnetic beads<sup>9</sup> have been reported to perform high-throughput immunodetection.

Poly(dimethylsiloxane) (PDMS) has become the most popular material with which to fabricate microfluidic devices for bioanalysis as this low-cost elastomer is easily molded into complex liquid channels and monolithically embedded valves for flow control.<sup>10</sup> Several PDMS devices have been applied to immunoassays. Detection using fluorescence images,<sup>11</sup> label-free surface plasmon resonance<sup>12</sup> or confocal imaging<sup>13</sup> provides excellent sensitivity but requires complicated or expensive

instrumentation. Highly sensitive detection of HIV and other antigens from multiple samples can be achieved in parallel through PDMS slabs with microchannels and proper substrate material for protein adsorption.<sup>14,15</sup>

Surface patterning is a practical and popular method that can easily be applied to many high-throughput and small-volume biological applications to create functional surfaces for controllable chemical reactions,<sup>16,17</sup> microarrays or spots of biomolecules,<sup>18,19</sup> and well orientated single molecules.<sup>20</sup> Many patterning approaches, including widely-used micro-contact printing,<sup>21–23</sup> have been reported to create colonies for cell culture and coculture,<sup>24,25</sup> cell transfection,<sup>26,27</sup> drug screening,<sup>24</sup> stem cell differentiation,<sup>28</sup> and many other studies based on single cells.<sup>29</sup> However, for most of these methods that pattern openly-accessible surfaces with limited integration and automation, careful operations are essential to eliminate contaminations.

Here we report a novel method to pattern the microfluidic channels through mechanical blocking *in situ*. With the simple and robustly-created patterns, our integrative microfluidic chip performs high-throughput fluorescence sandwich immunoassays using less than 1  $\mu$ l antibody solution and with a detection limit lower than 10 pg  $\text{mL}^{-1}$  for clinical samples.

The device, shown in Fig. 1, contains 32 reaction chambers for immunoassay detection in parallel. The volume of each chamber is 2 nL. The chip is made from PDMS through multi-layer soft lithography<sup>30</sup> on an epoxide glass slide. Each chamber has a round shape button valve, the critical component for chip function originated from the “MITOMI” chips.<sup>31</sup> The chambers are formed by segmenting microfluidic channels with a series of embedded pneumatic valves. These isolation valves can be divided into two major groups, longitudinal valves and horizontal ones. Each chamber is formed by two pairs of valves that isolate the button. When pressure is applied to the button, the deformable PDMS membrane will partially cover the channel since the button diameter is smaller than channel width. The activation of buttons does not block the liquid flow in the microfluidic channels completely. Therefore, only certain area in the channel is mechanically blocked, preventing liquid access. We have designed multiple inlets with gating valves to introduce common reagents, including washing buffer, blocking buffer, capture antibodies, and detecting antibodies. Samples are brought into the chip through another set of inlets. Each reaction chamber needs only a few

<sup>a</sup>College of Engineering, Peking University, Beijing, 100871, China.  
E-mail: yanyi@pku.edu.cn (Y.H.); gez@pku.edu.cn (Z.G.)

<sup>b</sup>Biodynamic Optical Imaging Center (BIOPIC), Peking University, Beijing, 100871, China

<sup>c</sup>Beijing Shijitan Hospital, Capital Medical University, Beijing, 100038, China

† Electronic Supplementary Information (ESI) available: Experimental details and supporting figures. See DOI: 10.1039/c2lc40145b/

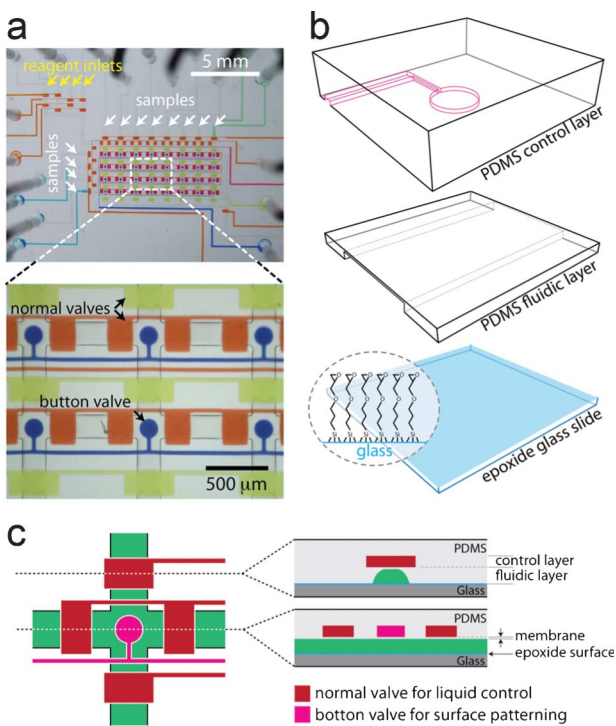


**Fig. 1** The microfluidic immunoassay chip and the construction of the button valves. (a) The microphotographs of a chip with inlets for introducing reagents and samples. Normal valves are used to create the small reaction chambers, while the button valves are used to pattern the epoxide surface. The chip is filled with dyes to illustrate different layers. (b) The layered structure of the device. (c) The top-view and side-views of a reaction chamber unit.

nanoliter solutions for each step of the experiment, with a total consumption of antibody solution less than 1  $\mu$ l for most reactions.

The workflow of immunoassay on-chip is shown in Fig. 2. For sandwich immunoassay, we first activated the buttons to protect the reaction spots, and then incubated the whole channel with bovine serum albumin (BSA) based blocking buffer. In the blocking buffer accessible region, the proteins reacted covalently

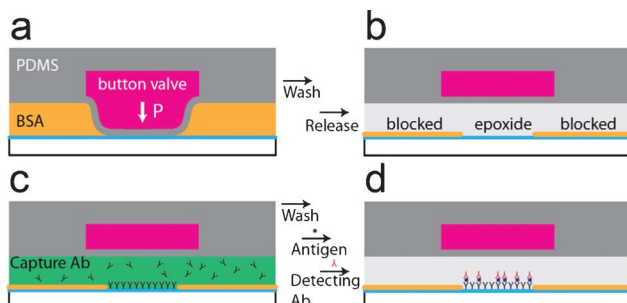


**Fig. 2** Workflow of the device and pattern formation. (a) Under pressure, the bottom PDMS membrane of the button deforms and partially blocks the channel. When the BSA blocking buffer is introduced into the channel, the uncovered surface will be blocked. (b) After releasing the button, the previously protected pattern becomes reactive sites. (c) During the sandwich fluorescence ELISA, the mechanically patterned reaction area is modified with capture antibody for antigen binding. (d) The detecting antibody selectively binds to antigen, leading to detectable fluorescence signal.

with epoxide to prevent further chemical modification on the slide. The excess blocking buffer was then flushed away by phosphate-buffered saline (PBS), the washing buffer. After releasing the buttons, the protected regions with intact epoxide groups were exposed. We bonded the capture antibody to the mechanically patterned spots by incubating with antibody solution (500  $\mu$ g ml<sup>-1</sup>) for 15 min. After another PBS washing, we added the sample for binding. We employed the Fluorescein isothiocyanate (FITC)-conjugated detecting antibody and detected the fluorescence signal coming out of the patterned spots. We carried out our detection using a fluorescence microscope equipped with a CCD camera. Excited with blue light at 490 nm, the green emission (520 nm) of the chip was imaged and then analyzed with Image J.<sup>32</sup> The intensity of the serum-blocked areas, generated from non-specific binding, was used for background subtraction. Compared with previous approaches using controllable microfluidic devices, the major advantage of our design is that the patterned spots provide identical reaction conditions for all tests on-chip, with fixed location of each spot for signal detection and the adjacent area for background correction.

The buttons are circular in design so that pressure is distributed symmetrically. The size of the reaction area patterned by the buttons is mainly decided by the pressure applied (Fig. S1†). Over-pressurized (>0.25 MPa) buttons will interfere with liquid flow, while under-pressurized (<0.05 MPa) buttons block insufficient portions of the channels and the patterning is less stable, leading to low sensitivity and reproducibility.

Protein-surface binding is a key factor for sandwich immunoassays. Although physical adsorption of protein molecules on PDMS surface have been applied to immunodetection,<sup>13</sup> we find that epoxide-reactive glass substrates are still the optimal choice. We use FITC-conjugated human IgG to compare the binding performances of PDMS and that of epoxide glass substrates (Fig. S2a†). PDMS offers similar detection limits as the epoxide slide does, but the irreversible covalent attachment of proteins on the epoxide surface provides better robustness and controllability than the reversible van der Waals interactions between proteins and the PDMS surface.<sup>33,34</sup>

During the patterning process, blocking buffer covers whole surface except the patterns protected by actuated buttons. Formulation of the blocking buffer affects the fluorescent background. We have tested four formulas: PBS, PBS with 1% BSA, PBS with 1% BSA and 10 mM Tris buffered saline, and PBS with 1% BSA and 20% polyethylene glycol (PEG-2000). We incubated the micro-channels with blocking buffer for 10 min, and then with FITC-labeled goat anti-human IgG for 15 min. Fluorescence images show that BSA indeed blocks the surface and Tris is essential to facilitate the blocking performance and to lower the background (Fig. S2b†). We found that the reaction buffer is also critical to the performance of sandwich immunoassays. Carbonate buffer solution (CBS, pH 9.6) ensures stable coupling between proteins and epoxide glass slides (Fig. S2c†) and generate more stable conditions for immunoassays. We found that 15 min is sufficient for stable binding between proteins and substrates. Over-adsorption may introduce artifacts into the concentration determination (Fig. S2d†). The concentration of capture antibody is highly related to the detection limit in our sandwich immunoassay (Table S1†). The higher the concentration of capture antibody, the lower the detection limit. Therefore, we

can design the proper protocol to match the sensitivity and dynamic range required for detecting specific antigens. We chose  $500 \mu\text{g ml}^{-1}$  capture antibody and reached the detection limit as low as  $0.02 \mu\text{g ml}^{-1}$ .

Proper concentration of detecting antibody is determined by checkerboard titration (Fig. S3†). The concentration should be high enough to boost the sensitivity of the immunoassay. However, high concentration will directly lead to high background intensity, resulting in unreliable measurement of antigen at low concentration. We found that  $125 \mu\text{g ml}^{-1}$  detecting antibody solution provided proper balance between sensitivity and background intensity.

Through these trials the final experimental protocol has been optimized. The whole experiment is performed at  $25^\circ\text{C}$ . We first blocked non-reactive areas with blocking buffer (PBS with 1% BSA and 10 mM Tris buffered saline) for 10 min with the button activated. After PBS washing, the buttons were inactivated and the unprotected button area is treated with  $500 \mu\text{g ml}^{-1}$  capture antibody for 15 min. After another PBS washing, we introduced the sample and incubated for 15 min. We then washed the channels with PBS, and incubated the channels with  $125 \mu\text{g ml}^{-1}$  detecting antibody for 10 min. The images were taken after the final PBS washing.

The performance of the chip is firstly evaluated by FITC-conjugated human IgG through a direct binding assay. After the blocking step, all buttons were released and the proteins with different concentrations were injected into channels to react with the pattern with epoxide groups exposed. The linear relationship between the spot intensity and the FITC-IgG concentration is shown in Fig. 3, with a dynamic range over  $10^4$ . Since direct binding assay was usually not reliable enough for immunodetection, we then tested the performance of sandwich immunoassay using this device by coupling the mouse anti-human IgG monoclonal antibody onto the epoxide spots, capturing human IgG (antigen) with different concentrations, and then using FITC-conjugated rabbit anti-human IgG polyclonal antibody as the detecting antibody to measure the fluorescence intensity of each spot (Fig. S4†). The chip could perform with a detection limit as low as  $1 \mu\text{g ml}^{-1}$ , with a linear dynamic range from  $1 \mu\text{g ml}^{-1}$  to  $10 \text{ ng ml}^{-1}$  (Fig. 3c). This range is ideal for many biomarkers detection at physiologically relevant concentrations.

We designed an improved version of the device, with more reaction chambers (Fig. S5†), for sandwich immunoassay detection of carcinoembryonic antigen (CEA) from human serum samples. Elevated CEA levels in human serum ( $>2.5 \text{ ng ml}^{-1}$ ) can serve as a diagnostic marker for colon, lung and breast cancers.<sup>35</sup> Fast and sensitive measurement of CEA level can facilitate the early detection of cancers. We chose mouse anti-human CEA monoclonal antibody as capture antibody, and rabbit anti-human CEA polyclonal antibody as detection antibody. Results (Fig. 4) show the linear dynamic range from  $10 \text{ pg ml}^{-1}$  to  $1 \mu\text{g ml}^{-1}$ . Six serum samples from patients were used for analyzing CEA level with our immunoassay chip. Fig. 4b shows the images of button spots and different samples had different fluorescence intensities. The result of our approach agrees very well with the control experiments performed with conventional sandwich immunoassay using microwell-plates. The error bars of our chip-based measurement are smaller than those of conventional method, indicating the excellent robustness and reproducibility of this chip-based device

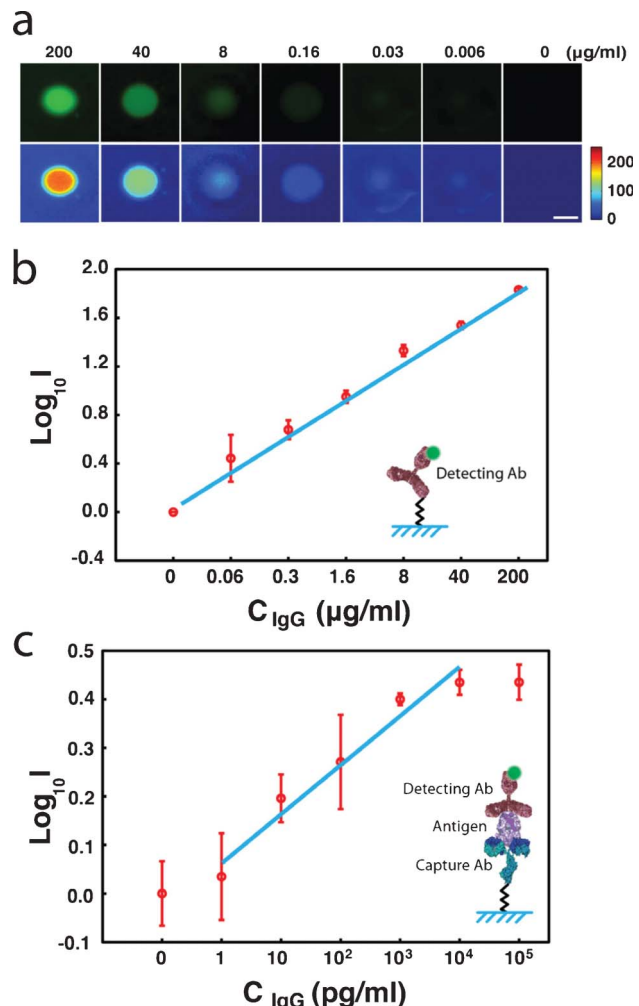


**Fig. 3** The immunoassay result using model systems. (a) The fluorescence images of FITC–human IgG coupled onto the mechanically patterned substrate. The upper row is the original images and the lower row is the corresponding color map of the intensity. Scale bar is  $100 \mu\text{m}$ . (b) The fluorescence intensity is linearly related to IgG concentration ( $n = 3$ ). (c) The fluorescence sandwich immunoassay detection of human IgG antigen ( $n = 3$ ) at different concentrations. The data presented in (b) and (c) are background subtracted.

( $\text{CV} = 10\%$ ). Moreover, in contrast with the conventional  $20 \mu\text{l}$  sample consumption for a single test and  $6 \text{ h}$  experimental time, our method requires less than  $1 \mu\text{l}$  serum for four experimental replicates in parallel, and finishes the assay within  $1 \text{ h}$ . This reduction of experimental time, due to the highly confined volume of reaction, greatly facilitates the sandwich immunoassay application in clinical diagnostics and point-of-care testing, and it has the potential to become a routine, rapid biochemical analysis technique.

In conclusion, we have developed a novel microfluidic device to perform high-throughput ELISA measurements with mere  $1 \mu\text{l}$  of each sample for four repeats, and a  $1 \text{ h}$  total experimental time. The reaction pattern created by mechanical protection efficiently binds the capture antibodies, offering reliable and robust substrate to perform sandwich fluorescence ELISA. We have achieved a linear dynamic range over 5 logs and the detection limit at  $10 \text{ pg ml}^{-1}$  for CEA measurement. Applying our method to serum

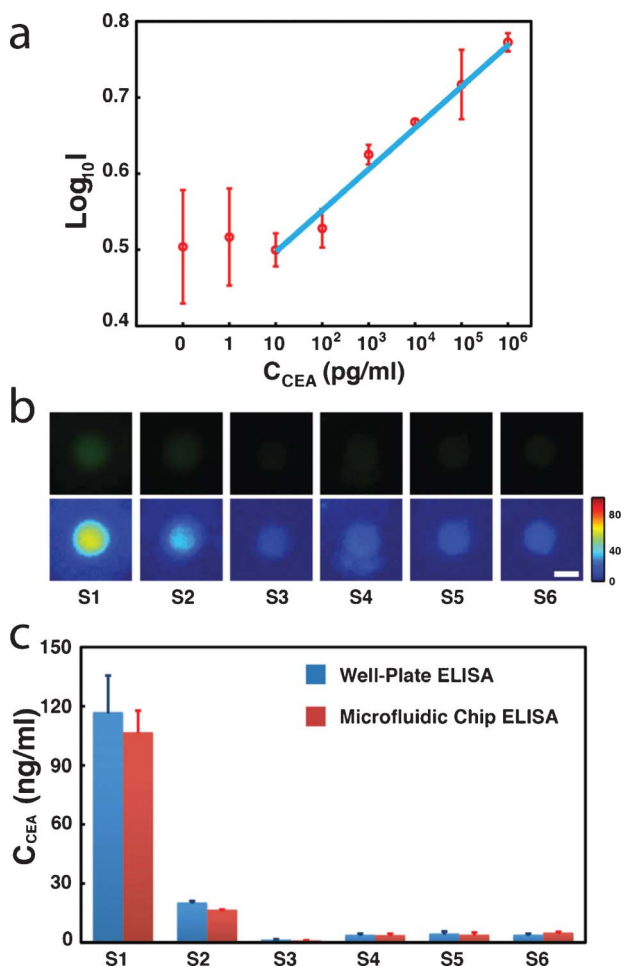


**Fig. 4** The sandwich immunoassay of CEA. (a) The sandwich immunoassay of standard CEA samples with different concentration. (b) The fluorescence images (upper row) and processed color maps (lower row) of 6 patient serum samples. Scale bar is  $100 \mu\text{m}$ . (c) The measured CEA concentration using both chip-based and conventional sandwich immunoassays ( $n = 3$ ).

samples from patients, we have reached comparable results with conventional assays, with improved reproducibility and greatly reduced sample consumption. The dynamic range, the detection limit, the low consumption of sample and reagents, as well as the short time needed for measurement of this chip-based method meet the general requirements of clinical diagnostics. We envision that this method has great potential for high-throughput immunoassays and controllable surface patterning.

## Acknowledgements

This research was supported by grants from the National Natural Science Foundation of China (20890020 and 90913011 to Y. H.; 20905004 to Y.P.), the Ministry of Science and Technology of China (200GAA042309 and 2011CB809106 to Y.H.), the Fok Ying Tung Educational Foundation to Y. H., and the Novo Nordisk-CAS Research Foundation (NNCAS-2010-5) to Z. G.

## References

- 1 C. D. Chin, T. Laksanasopin, Y. K. Cheung, D. Steinmiller, V. Linder, H. Parsa, J. Wang, H. Moore, R. Rouse, G. Umviligihozo, E. Karita, L. Mwambarangwe, S. L. Braunstein, J. van de Wijgert, R. Sahabo, J. E. Justman, W. El-Sadr and S. K. Sia, *Nat. Med.*, 2011, **17**, 1015–1019.
- 2 R. M. Lequin, *Clin. Chem.*, 2005, **51**, 2415–2418.
- 3 B. S. Ferguson, S. F. Buchsbaum, T. T. Wu, K. Hsieh, Y. Xiao, R. Sun and H. T. Soh, *J. Am. Chem. Soc.*, 2011, **133**, 9129–9135.
- 4 B. Zheng, L. S. Roach and R. F. Ismagilov, *J. Am. Chem. Soc.*, 2003, **125**, 11170–11171.
- 5 L. F. Cheow, S. H. Ko, S. J. Kim, K. H. Kang and J. Han, *Anal. Chem.*, 2010, **82**, 3383–3388.
- 6 W. T. Liu, L. Zhu, Q. W. Qin, Q. Zhang, H. Feng and S. Ang, *Lab Chip*, 2005, **5**, 1327–1330.
- 7 J. C. McDonald, S. J. Metallo and G. M. Whitesides, *Anal. Chem.*, 2001, **73**, 5645–5650.
- 8 B. S. Lee, Y. U. Lee, H. S. Kim, T. H. Kim, J. Park, J. G. Lee, J. Kim, H. Kim, W. G. Lee and Y. K. Cho, *Lab Chip*, 2011, **11**, 70–78.
- 9 G. Acharya, C. L. Chang, D. D. Doorneweer, E. Vlashi, W. A. Henne, L. C. Hartmann, P. S. Low and C. A. Savran, *J. Am. Chem. Soc.*, 2007, **129**, 15824–15829.
- 10 T. Thorsen, S. J. Maerkel and S. R. Quake, *Science*, 2002, **298**, 580–584.
- 11 E. P. Kartalov, J. F. Zhong, A. Scherer, S. R. Quake, C. R. Taylor and W. F. Anderson, *BioTechniques*, 2006, **40**, 85–90.
- 12 Y. Luo, F. Yu and R. N. Zare, *Lab Chip*, 2008, **8**, 694–700.
- 13 J. Kong, L. Jiang, X. Su, J. Qin, Y. Du and B. Lin, *Lab Chip*, 2009, **9**, 1541–1547.
- 14 X. Jiang, J. M. Ng, A. D. Stroock, S. K. Dertinger and G. M. Whitesides, *J. Am. Chem. Soc.*, 2003, **125**, 5294–5295.
- 15 D. Yang, X. Niu, Y. Liu, Y. Wang, X. Gu, L. Song, R. Zhao, L. Ma, Y. Shao and X. Jiang, *Adv. Mater.*, 2008, **20**, 4770–4775.
- 16 Y. X. Chen, G. Triola and H. Waldmann, *Acc. Chem. Res.*, 2011, **44**, 762–773.
- 17 X. Zhou, F. Boey, F. Huo, L. Huang and H. Zhang, *Small*, 2011, **16**, 2273–2289.
- 18 T. Ekblad and B. Liedberg, *Curr. Opin. Colloid Interface Sci.*, 2010, **15**, 499–509.
- 19 A. Calabretta, D. Wasserberg, G. A. Posthuma-Trumpie, V. Subramaniam, A. v. Amerongen, R. Corradini, T. Tedeschi, S. Sforza, D. N. Reinhoudt, R. Marchelli, J. Huskens and P. Jonkheijm, *Langmuir*, 2011, **27**, 1536–1542.
- 20 A. Cerf, B. R. Cipriany, J. J. Benitez and H. G. Craighead, *Anal. Chem.*, 2011, **83**, 8073–8077.
- 21 J. L. Wilbur, A. Kumar, H. A. Biebuyck, E. Kim and G. M. Whitesides, *Nanotechnology*, 1996, **7**, 452–457.
- 22 A. Perl, D. N. Reinhoudt and J. Huskens, *Adv. Mater.*, 2009, **21**, 2257–2268.
- 23 J. C. Love, L. A. Estroff, J. K. Kriebel, R. G. Nuzzo and G. M. Whitesides, *Chem. Rev.*, 2005, **105**, 1103–1169.
- 24 S. R. Khetani and S. N. Bhatia, *Nat. Biotechnol.*, 2008, **26**, 120–126.
- 25 L. Li, J. R. Klim, R. Derda, A. H. Courtney and L. L. Kiessling, *Proc. Natl. Acad. Sci. U. S. A.*, 2011, **108**, 11745–11750.
- 26 D. B. Wheeler, A. E. Carpenter and D. M. Sabatini, *Nat. Genet.*, 2005, **37**, S25–S30.
- 27 H. Zhang, Y. Hao, J. Yang, Y. Zhou, J. Li, S. Yin, C. Sun, M. Ma, Y. Huang and J. J. Xi, *Nat. Commun.*, 2011, **2**, 554.
- 28 A. Chaubey, K. J. Ross, R. M. Leadbetter and K. J. L. Burg, *J. Biomed. Mater. Res., Part B*, 2008, **84B**, 70–78.
- 29 G. M. Whitesides, E. Ostuni, S. Takayama, X. Jiang and D. E. Ingber, *Annu. Rev. Biomed. Eng.*, 2001, **3**, 335–373.
- 30 M. A. Unger, H. P. Chou, T. Thorsen, A. Scherer and S. R. Quake, *Science*, 2000, **288**, 113–116.
- 31 S. J. Maerkel and S. R. Quake, *Science*, 2007, **315**, 233–237.
- 32 T. J. Collins, *BioTechniques*, 2007, **43**, 25–30.
- 33 J. C. McDonald, D. C. Duffy, J. R. Anderson, D. T. Chiu, H. Wu, O. J. Schueler and G. M. Whitesides, *Electrophoresis*, 2000, **21**, 27–40.
- 34 S. Y. Seong, *Clin. Diagn. Lab. Immunol.*, 2002, **9**, 927–930.
- 35 N. Laboria, A. Fragoso, W. Kemmner, D. Latta, O. Nilsson, M. Luz Botero, K. Drese and C. K. O'Sullivan, *Anal. Chem.*, 2010, **82**, 1712–1719.